

Joint Mobile IAB Node Positioning and Scheduler Selection in Locations With Substantial Obstacles

Paulo Furtado Correia, André Coelho, Manuel Ricardo
INESC TEC, Faculdade de Engenharia, Universidade do Porto, Portugal
{paulo.j.correia, andre.f.coelho, manuel.ricardo}@inesctec.pt

Abstract— Integrated Access and Backhaul (IAB) in cellular networks combines access and backhaul within a wireless infrastructure reducing reliance on fibre-based backhaul. This enables faster and more cost-effective network expansion, especially in hard-to-reach areas. Positioning a mobile IAB node (MIAB) in a seaport environment, in order to ensure on-demand, resilient wireless connectivity, presents unique challenges due to the high density of User Equipments (UEs) and potential shadowing effects caused by obstacles. This paper addresses the problem of positioning MIABs within areas containing UEs, IAB donors (CFs), and obstacles. Our approach considers user associations and different types of scheduling, ensuring MIABs and CFs meet the capacity requirements of a special team of served UEs, while not exceeding backhaul capacity. Using Genetic Algorithm (GA) solver, we achieve capacity improvement gains, by up to 200% for the 90th percentile. The proposed solution improves network performance, particularly during emergency capacity demands.

Keywords— 3D obstacle shadowing; 6G; Cell selection; IAB node; Scheduling; Seaport communications; Wireless backhaul.

I. INTRODUCTION

Key societal sectors are becoming increasingly digitalised and data-driven. Sixth-generation (6G) networks aim at bridging the digital and physical worlds, providing resilient wireless connectivity to diverse verticals, including critical sectors such as seaports. These industrial environments have to enable communications between human operators, machinery equipment, sensors and video cameras, throughout their operational areas. In a seaport, the areas include terrestrial and nearshore locations, where operations take place. Container yards handle vast metallic loads with ships, cranes, and trucks in an increasingly automated environment. A well-designed 6G wireless network, with adequately positioned cells, capable of providing the network capacity demanded by port users, is a promising solution for these environments. Moreover, it would benefit from MIABs carried by terrestrial vehicles or Unmanned Aerial Vehicles (UAVs). They can be used to cover obstructed areas and provide extra capacity, such as for emergency or rescue teams.

In this paper, we investigate the added value of deploying an MIAB in a container yard at a seaport. We assume the following: 1) the seaport is covered by a set of CFs where obstacles, such as piles of containers, may severely attenuate the radio signal in certain zones; 2) the MIAB's backhaul link is wireless, established via the NR Uu interface to an available IAB donor (CF); 3) the MIAB is carried by a terrestrial vehicle, which may move throughout the seaport; 4) the MIAB aims to improve the communications provided to a specific group of users, called the special team. The focus is on the positioning of the MIAB within the port and exclude networking architectural aspects, which could benefit from the

latest solutions proposed by 3GPP [19]. Hence, radio coverage must be optimised to maximise network capacity, thereby enhancing communications efficiency and boosting the overall productivity of services within Smart Ports [1], such as emergency assistance truck rolls by special teams of users within individual areas.

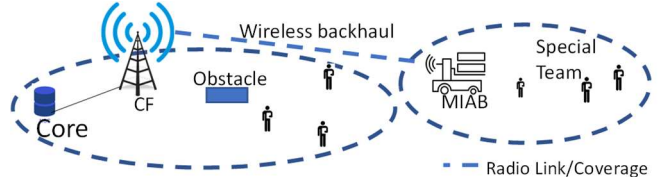


Fig. 1 – Concept diagram describing a CF connected to a MIAB through its wireless backhaul, both providing coverage to a set of UEs located in well-delimited areas, subject to shadowing caused by obstacles.

This paper provides the following original contributions:

1) *A model for positioning MIABs and selecting the access and backhaul scheduler, in a 3D obstacle-aware environment.* We formulate the problem of positioning the MIABs considering the presence of CFs, substantial obstacles, areas where the MIAB can move, and a set of users requiring improved network performance. Additionally, the model considers two radio resource scheduling techniques - Round Robin (RR) and Proportional Fair (PF) to determine the position for the MIABs that maximise the aggregate network capacity offered to a special team. For instance, commanders of first response team or personnel or equipment involved in a localised, temporary rescue or civil work.

2) *Network performance evaluation.* We evaluate the performance of the access and backhaul wireless network considering randomly generated scenarios at Terminal XXI, Port of Sines, Portugal, as shown in Fig. 1. The port is divided into geographical well-delimited areas.

The remainder of this paper is structured as follows. Section II reviews the related work on positioning MIABs in outdoor areas, considering obstacles affecting the access and backhaul, cell selection, and scheduling algorithms. Section III describes the system model, including the methodology adopted, the main constraints, and the performance metrics employed. Section IV presents the performance evaluation study and discusses the results obtained. Finally, Section V summarises the key findings and proposes directions for future work.

II. RELATED LITERATURE

Operations in seaports involving containers, trucks, ships, or cranes can cause shadowing, degrading the performance of legacy networks. In [3], wireless link disruptions caused by obstacles are mitigated through proactive handovers by considering links' history and their disruption probabilities. In

[4], for the same type of mitigation, blockages are predicted using deep-learning. Both solutions are non-deterministic. Computer vision can also predict obstacles, users and their velocities, aiding in timely handovers as in [5], [6]; however, these solutions have low accuracy in non-line-of-sight (NLoS) and low-luminosity conditions. In [7], computer vision aided by Machine Learning creates bounding boxes of obstacles to predict imminent blockages of wireless links; the accuracy of this solution is limited by the video cameras' resolution and the distances between objects. In [8], objects are modelled by cuboids and the NLoS conditions deterministically calculated using geometrical analysis; however, obstacles are reduced to zero-volume single points. Regarding the backhaul link, multiple solutions are provided in the literature. In [9], a solution is proposed for positioning of a mobile cell deployed in a UAV, considering also terrestrial base stations; this solution maximises the sum-rate but ignores obstacle shadowing in the backhaul link. [10] proposes a solution for drone-cells positioning, considering the constraints of backhaul capacity; however, it maximises the number of covered users rather than their sum-capacity. [11] considers the backhaul link to maximise total network capacity for UAV base station positioning and channel allocation. [12] addresses the same problem but considers a free-space optical link for the backhaul; still, none of these solutions consider obstacles. [13] maximises the downlink sum-rate by controlling radio resources, transmission powers and UAV placement; this solution is backhaul-aware but still do not consider obstacle blockages. Optimal placement of base stations, given UEs' coordinates, is also considered in [14] for the minimum network cost conditions; however, it ignores obstacles and backhaul requirements.

The literature provides solutions for base station positioning aimed at optimising various criteria, considering factors such as obstacle shadowing, cell selection procedures, backhaul capacity, resource allocation and scheduling algorithms. Nonetheless, to our knowledge, no published work addresses non-mmWave MIAB positioning to maximise network capacity for UEs in a defined area, whilst simultaneously accounting for obstacle shadowing, backhaul capacity, cell selection, resource allocation, and scheduling.

III. SYSTEM MODEL

Let us consider a three-dimensional networking scenario, as depicted in Fig. 2, where M MIABs must be positioned within a given area of the seaport. The MIABs aim at providing wireless connectivity to a special team of S UEs out of the total U , initially served by F CFs. The environment includes obstacles that may disrupt the access or backhaul wireless links. The objective is to position the MIABs and determine their user associations with all UEs to maximise the aggregate network capacity offered to the special team within a given area. Additionally, each MIAB's backhaul must support the capacity of the UEs it serves. In order to achieve this, the Euclidean coordinates for placing the MIABs (x_m^M, y_m^M, z_m^M) and the corresponding user associations ($S_{j,m}^M$) are determined to maximise the objective function.

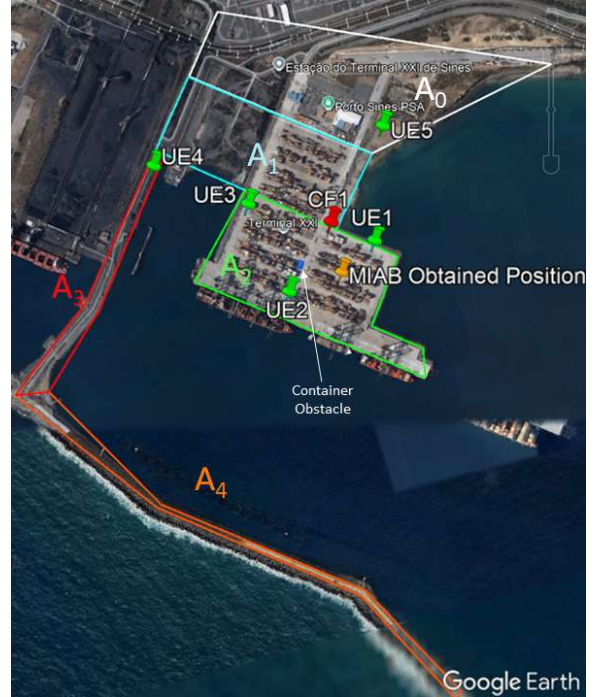


Fig. 2 - A top-down view of Sines Port's Terminal XXI in Portugal, with candidate deployment areas (A_0 - A_4) for MIABs. CF1 (red marker) connected to a MIAB (orange marker) through its wireless backhaul, both providing coverage to UEs (UE1-UE5) located in well-defined areas, subject to potential shadowing from substantial obstacles.

A. Problem Formulation

The problem is formulated as a Mixed-Integer Nonlinear Programming (MINLP) problem. The variables used to formulate the problem and their definitions are presented in Table I. The objective function in (1) maximises the sum of the network capacities offered to the S UEs, ensuring single associations as denoted by (2). The 2D distances defined in (3), along with the applicable spectral efficiencies in (4), follow the models in [15]-[17]. For each access and backhaul wireless link, constraints (3) and (4) apply. The problem formulation is made generic, applicable to scenarios with F CFs and M MIABs, each MIAB having a wireless backhaul to a single CF, as ensured by constraint (5). The aggregate capacity must satisfy constraint (7), where each MIAB's backhaul capacity ($C_{m,k}^F$) must meet or exceed the sum of the capacities offered to the UEs the MIAB serves. Moreover, each wireless link's Reference Signal Received Power (RSRP) must exceed a minimum threshold ($qRxLevMin$), according to constraint (6), adapted from [2] to our scenario.

$$\max_{x_m^M, y_m^M, z_m^M, S_{u,m}^M, S_{u,k}^F, S_{m,k}^F} \sum_{u \in S} (\sum_{m \in M} (C_{u,m}^M S_{u,m}^M) + \sum_{k \in F} (C_{u,k}^F S_{u,k}^F)) \quad (1)$$

subject to:

$$\sum_m S_{u,m}^M + \sum_k S_{u,k}^F = 1, \forall u \in [1, U], \forall m \in [1, M], \forall k \in [1, F] \quad (2)$$

$$10 \leq d_{2Du,m}^M, d_{2Du,k}^F, d_{2Dm,k}^F \leq 5000 \quad (3)$$

$$0 \leq SE_{u,m}^M, SE_{u,k}^F, SE_{m,k}^F \leq 6.4 \quad (4)$$

$$\sum_k S_{m,k}^F = 1, \forall k \in [1, F] \quad (5)$$

$$R_{u,m}^M, R_{u,k}^F, R_{m,k}^F \geq qRxLevMin \quad (6)$$

$$C_{m,k}^F \geq \sum_{u \in U} (C_{u,m}^M S_{u,m}^M), \forall m \in [1, M] \quad (7)$$

$$x_m^M, y_m^M \in A_a, z_m^M = h_{BSm} = 5 \quad (8)$$

TABLE I. LIST OF THE MAIN NOTATIONS USED IN THE PROBLEM FORMULATION.

Notation	Definition
a, u, m, k	Indices representing area A , UE , $MIAB$ and CF .
$MIAB_m$	$MIAB$ m , where m ranges from 1 to M .
CF_k	Fixed IAB donor k , where k ranges from 1 to F .
UE_u	User equipment u , where u ranges from 1 to U .
S	Number of UEs of the special team ($S \leq U$).
A_a	The selected area A , where the special team requires capacity, as depicted in Fig.1. Each area is bounded by coloured lines defined by linear inequations.
$C_{u,m}^M, C_{u,k}^F, C_{m,k}^F$	Capacities provided respectively by $MIAB_m$ or CF_k to the UE_u , and CF_k to $MIAB_m$'s backhaul measured in bit/s.
B	Resource Blocks (RBs) used per numerology.
$\Delta fr_{1_m}, \Delta fr_{1_k}$	Subcarrier spacing (SCS) for $MIAB_m$, CF_k in Hz.
U_m, U_k	Number of UEs associated to $MIAB_m$, CF_k .
U_z	Number of RNTIs considered for RBs split, depending on the used scheduling type.
$S_{u,m}^M, S_{u,k}^F, S_{m,k}^F$	Binary variables indicating user association of UE_u to $MIAB_m$, CF_k , and $MIAB_m$'s backhaul association to CF_k (1 if associated, 0 otherwise).
$Bw_{u,m}^M, Bw_{u,k}^F$	Bandwidth of the channel respectively between UE_u and $MIAB_m$ or CF_k , in Hz.
$Bw_{m,k}^F$	Bandwidth of the backhaul between $MIAB_m$ and CF_k , in Hz.
$SINR_{u,m}^M, SINR_{u,k}^F$	SINR of the channel respectively between UE_u and $MIAB_m$ or CF_k , in dB.
$SINR_{m,k}^F$	Backhaul SINR between $MIAB_m$, CF_k in dB.
$R_{u,m}^M, R_{u,k}^F, R_{m,k}^F$	Reference Signal Received Power (RSRP) by UE_u respectively from $MIAB_m$ or CF_k , and RSRP by $MIAB_m$'s backhaul from CF_k in dB.
N_{fr1_m}, N_{fr1_k}	Thermal noise power for $MIAB_m$ or CF_k in dB.
P_t	Transmission power in dBm.
c	Speed of light in vacuum (3×10^8 m/s).
f_m^M, f_k^F	$MIAB_m$'s and CF_k 's carrier frequency in GHz.
x_m^M, y_m^M, z_m^M	Euclidean coordinates of $MIAB_m$ in m.
x_u^U, y_u^U, z_u^U	Euclidean coordinates of UE_u in m.
h_{BSm}, h_{BSK}, h_{UT}	$MIAB_m$'s, CF_k 's and UE_u 's heights in m. $h_{BSm} = 5$ m; $h_{BSK} = 10$ m; $h_{UT} = 1.5$ m, as [16].
$d_{2Du,m}^M, d_{3Du,m}^M$	2D and 3D Euclidean distances between UE_u and $MIAB_m$ in m.
$d_{BPu,m}^M$	2D Euclidean breakpoint distances between UE_u and $MIAB_m$ in m.
μ_{fr1_m}, μ_{fr1_k}	FR1's numerology used by $MIAB_m$ or CF_k .
$\eta_{u,m}^M, \eta_{u,k}^F, \eta_{m,k}^F$	Spectral efficiency of the established downlink RNTI respectively between UE_u and $MIAB_m$ or CF_k , or between $MIAB_m$ and CF_k in bit/s/Hz.
$SE_{u,m}^M, SE_{u,k}^F, SE_{m,k}^F$	Obtained regression for spectral efficiency of the established downlink RNTI between UE_u , $MIAB_m$ or CF_k , as per (18), a linear function of the respective $SINR$, in bit/s/Hz, [18].
$PL_{UMi_LOSu,m}^M, PL_{UMi_NLOSu,m}^M$	Path loss for UMi scenarios considered for LoS or NLoS link between UE_u and $MIAB_m$.
$qRxLevMin$	Minimum RSRP needed to provide positive capacity, adapted to current configurations (-122 dBm) [2].
$RB_{u,k}, RB_{u,m}, RB_{m,k}$	Number of RBs respectively between UE_u and CF_k or $MIAB_m$, and between $MIAB_m$ and CF_k .

The problem solver provides the following results: 1) the aggregate capacity available to the special team of S UEs; 2)

the user associations of all UEs to the cells, represented by binary variables indicating each UE's associated cell; and 3) the $MIAB$'s Euclidean coordinates adhering to (8). The capacities of the Radio Network Temporary Identifier (RNTI) between UE_u and either $MIAB_m$ and/or CF_k is defined in (9). It depends on several factors, including: 1) the spectral efficiency, defined in (10); 2) SCS, as defined in (11) for both frequencies; 3) the total number of RBs available and the number of UEs associated to a cell, which are allocated to connected UEs and backhauls; and 4) the scheduling type, PF or RR. PF allocates the RBs fairly among the U_k UEs connected directly, as well as the U_m UEs connected indirectly via $MIAB_m$'s backhaul, as specified in (12). RR treats the $MIAB_m$'s backhaul as a single UE and allocates the RBs fairly based on the number of wireless links to CF_k . The allocation depends on the sum of backhaul associations $S_{m,k}^F$ and the U_k UEs, as represented in (13).

$$C_{u,m}^M = \frac{B \Delta fr_{1_m} \eta_{u,m}^M}{U_m}; C_{u,k}^F = \frac{B \Delta fr_{1_k} \eta_{u,k}^F}{U_z}; \quad (9)$$

$$C_{m,k}^F = \begin{cases} \frac{B U_m \Delta fr_{1_k} \eta_{m,k}^F}{U_z}; & \text{PF scheduler} \\ \frac{B \Delta fr_{1_k} \eta_{m,k}^F}{U_z}; & \text{RR scheduler} \end{cases} \quad (9)$$

$$\eta_{u,m}^M = \begin{cases} SE_{u,m}^M, & SE_{u,m}^M \geq 0 \\ 0, & SE_{u,m}^M < 0 \end{cases}; \quad \eta_{u,k}^F = \begin{cases} SE_{u,k}^F, & SE_{u,k}^F \geq 0 \\ 0, & SE_{u,k}^F < 0 \end{cases} \quad (10)$$

$$\Delta fr_{1_m} = 2^{\mu_{fr1_m}} \cdot 15 \text{ kHz}; \quad \Delta fr_{1_k} = 2^{\mu_{fr1_k}} \cdot 15 \text{ kHz} \quad (11)$$

$$U_m = \sum_{u \in U} S_{u,m}^M; \quad U_k = \sum_{u \in U} S_{u,k}^F \quad (12)$$

$$U_z = \begin{cases} U_k + U_m; & \text{PF scheduler} \\ U_k + \sum_{m \in M} S_{m,k}^F; & \text{RR scheduler} \end{cases} \quad (13)$$

Hence, the number of RBs assigned for each access link to CF_k or $MIAB_m$ is respectively given by (14).

$$RB_{u,k} = \frac{B}{U_z}; \quad RB_{u,m} = \frac{B}{U_m} \quad (14)$$

Moreover, the number of RBs assigned to CF_k 's backhaul is determined by (15), depending on the scheduling type considered.

$$RB_{m,k} = \begin{cases} \frac{B U_m}{U_z}; & \text{PF scheduler} \\ \frac{B}{U_z}; & \text{RR scheduler} \end{cases} \quad (15)$$

The bandwidth used per RNTI for the direct wireless link between UE_u and either $MIAB_m$ or CF_k is given by (16). The bandwidth used by the backhaul of a CF_k is given by (17).

$$Bw_{u,m}^M = RB_{u,m} \Delta fr_{1_m}; \quad Bw_{u,k}^F = RB_{u,k} \Delta fr_{1_k} \quad (16)$$

$$Bw_{m,k}^F = RB_{m,k} \Delta fr_{1_k} \quad (17)$$

Equation (18) defines the spectral efficiency as a linear regression function of $SINR_{u,m}^M$, introduced, calibrated and demonstrated in [18], and validated in ns-3, as detailed in [17].

$$SE_{u,k}^F = 0.23 SINR_{u,k}^F - 0.21 \quad (18)$$

The same linear regression model is applied to $SE_{u,m}^M$ and $SE_{m,k}^F$, which represent the spectral efficiencies for the UEs and backhauls of $MIAB_m$, respectively, as a function of their

corresponding SINRs. This assumes the same MCS index table configuration is used for PDSCH, including modulation order, target code rate and corresponding spectral efficiency, as outlined in [15]. Applying (18) analogously in (10), results in spectral efficiencies $\eta_{u,m}^M$, $\eta_{u,k}^F$ and $\eta_{m,k}^F$, all of which positive.

The SINRs for each RNTI and the backhaul, in the absence of interference, are given by (19) and (20).

$$SINR_{u,m}^M = 10 \log_{10} \left(\frac{R_{u,m}^M}{N_{fr1_m}} \right); SINR_{u,k}^F = 10 \log_{10} \left(\frac{R_{u,k}^F}{N_{fr1_k}} \right) \quad (19)$$

$$SINR_{m,k}^F = 10 \log_{10} \left(\frac{R_{m,k}^F}{N_{fr1_k}} \right) \quad (20)$$

The received power and thermal noise power for each RNTI and the backhaul are respectively provided by (21), (22) and (23), depending on LoS or NLoS conditions, which are determined by obstacle shadowing. In (21), U_m is replaced by U_z for the analogous $R_{u,k}^F$ and $R_{m,k}^F$ equations, depending on the type of scheduling used.

$$R_{u,m}^M = \begin{cases} \frac{10 \left(\frac{P_t - 30}{10} \right)}{U_m PL_{UMi_LoSu,m}^M} ; \text{ if LoS} \\ \frac{10 \left(\frac{P_t - 30}{10} \right)}{U_m PL_{UMi_NLoSu,m}^M} ; \text{ if NLoS} \end{cases} \quad (21)$$

$$N_{fr1_m} = 10^{[-19.9 + \log_{10}(B \Delta f r1_m)]} \quad (22)$$

$$N_{fr1_k} = 10^{[-19.9 + \log_{10}(B \Delta f r1_k)]} \quad (23)$$

The RSRP in (21) relies on the 3GPP path loss model for a UMi scenario. In this model, CF_k cells are positioned at a height of 10 m, while $MIAB_m$ is at a height of 5 m, as specified in [16]. As such, the problem becomes a true 3D optimisation, considering different heights among cells, UEs and obstacles. The path loss depends on (24) and (25). Equation (24), applied to LoS conditions, represents a two-branch function with a non-linearity point at a 2D breakpoint distance between UEs and cells. For NLoS conditions, it equals the maximum of (24) and (25), as shown by (26). Similar path loss expressions can be derived for $PL_{UMi_LOSu,k}^F$, $PL_{UMi_LOSm,k}^F$, $PL_{UMi_NLOSu,k}^F$ and $PL_{UMi_NLOSm,k}^F$.

$$PL_{UMi_LOSu,m}^M = \begin{cases} PL_{1u,m}^M, \quad 10 \text{ m} \leq d_{2Du,m}^M \leq d_{BPu,m}^M \\ PL_{2u,m}^M, \quad d_{BPu,m}^M \leq d_{2Du,m}^M \leq 5 \text{ km} \end{cases} \quad (24)$$

$$PL_{UMi_NLOSu,m}^M = 10^{2.24} \frac{d_{3Du,m}^{3.53} f_m^{M2.13}}{10^{(0.03(h_{UT}-1.5)}}} \quad (25)$$

$$PL_{UMi_NLOSu,m}^M = \max(PL_{UMi_LOSu,m}^M, PL_{UMi_NLOSu,m}^M) \quad (26)$$

According to the definition in [16], $PL_{UMi_LOSu,m}^M$, as in (24), is represented by $PL_{1u,m}^M$ for 2D distances below the breakpoint distance and takes the values of $PL_{2u,m}^M$ for 2D distances above, as presented in (27) and (28), respectively.

$$PL_{1u,m}^M = 10^{3.24} d_{3Du,m}^{2.1} f_m^{M2} \quad (27)$$

$$PL_{2u,m}^M = 10^{3.24} \frac{d_{3Du,m}^{4} f_m^{M2}}{(d_{BPu,m}^M)^2 + (h_{BS} - h_{UT})^2}^{0.95} \quad (28)$$

In UMi scenarios, the 2D breakpoint distance between a transmitter and receiver is a function of their antenna heights, the probability of LoS, the effective environment height (h_E) and the carrier frequency used, as shown in (31). h_E is set to 1

m, with LoS probability of $1/(1+C(d_{2Du,m}^M, h_{UT}))$, which equals 1 for UEs' heights (h_{UT}) up to 13 m.

The model excludes path loss values for 2D distances greater than 5000 m, which are beyond the range considered for V , and less than 10 m, as ensured by optimisation constraint (3). The distances $d_{3Du,m}^M$, $d_{2Du,m}^M$ and $d_{BPu,m}^M$ are given by (29), (30) and (31), respectively. Analogous equations can be inferred for distances involving CF_k , such as access and backhaul, where the Euclidean coordinates, heights and frequencies of the parties involved are applied.

$$d_{3Du,m}^M = \sqrt{(x_m^M - x_u^U)^2 + (y_m^M - y_u^U)^2 + (z_m^M - z_u^U)^2} \quad (29)$$

$$d_{2Du,m}^M = \sqrt{(x_m^M - x_u^U)^2 + (y_m^M - y_u^U)^2} \quad (30)$$

$$d_{BPu,m}^M = \frac{4(h_{BS} - h_E)(h_{UT} - h_E) f_m^M 10^9}{c} \quad (31)$$

In NR, the SCS for FR1, as referred to in (11), and the numerology $\mu_{fr1} = 1$ result in a bandwidth of 30 kHz per RB. With 9 sub-carriers per RB used for data (the remaining 3 are used for control) and 133 RBs per slot, considering numerology 1, the total bandwidth available for data transmission is calculated as $133 \times 9 \times 30 \text{ kHz} = 35.9 \text{ MHz}$. The binary variables $S_{u,m}^M$, $S_{u,k}^F$ and $S_{m,k}^F$, in constraints (2) and (5), ensure single UE_u or backhaul associations with each cell. Constraint (3) ensures a lower bound 2D distance of 10 m respectively between UE_u and $MIAB_m$ or CF_k , and the backhaul, so the 3GPP path loss PL_1 applicability range in [16] is valid. Constraint (4) bounds the spectral efficiency, as defined in [17], based on Table 2 of EESM NR error model type with Chase Combining. In the frequency domain, we use 9 sub-carriers per RB instead of 12, while in the time domain we use 12 OFDM symbols per slot, rather than 14 to account for overhead. Therefore, the upper bound of the spectral efficiency is 6.4 (bit/s/Hz) instead of 7.4 (for MCS index 27 and modulation order 8), according to [15] and [17].

B. Obstacle-aware modelling

In order to solve the MIABs' positioning problem, we consider obstacles such as containers, trucks, cranes or ships. For that purpose, we model obstacles as trapezoidal cuboids, with six planar faces and eight vertices defined by their Euclidean coordinates. The procedure deterministically and geometrically identifies any intersection point between one or more faces of an obstacle and the line connecting any UE_u to either cell, or between two different cells connected by a wireless backhaul. The positions of UEs and cells are identified by their Euclidean coordinates, while the obstacle faces are defined by their vertices' coordinates and respective connecting lines' distances. For simplicity, the calculations to determine LoS or NLoS conditions are not presented herein. Moreover, NLoS conditions do not account for the specific attenuation introduced by the obstacle material. Hence, for any line considered, zero (LoS) or more (NLoS) intersection points with the face(s) of the obstacle(s) are identified. This implies using (24) for LoS or (26) for NLoS, as applied in (21).

IV. PERFORMANCE EVALUATION

In order to evaluate the proposed model for positioning an MIAB in a 3D obstacle-aware environment, we defined a set of scenarios and evaluated the corresponding network performance by running the Genetic Algorithm (GA) solver in MATLAB. After each run, the solver provided several results, including: the aggregate capacity for the special team of UEs

(UE1 and UE2), the gain compared with a baseline scenario, the user associations of UEs with the cells, the backhaul capacity of the MIAB, and the MIAB's position. The variants $V0$ to $V5$ and the evaluated metrics are presented in Fig. 3. The baseline variant $V0$ consisted of five UEs, all associated to CF_1 . Two of these formed the special team, within each area A_a , while the other three could be in any area. The special team and CF_1 were randomly positioned in each area A_a . $V0$ has a single CF and no MIAB. We also defined five variants of the $V0$ baseline – $V1$ to $V5$, with an MIAB to assist CF_1 . In $V1$, we added obstacles to $V0$; in $V2$ and $V3$, we used PF scheduling, respectively without and with obstacles; in $V4$ and $V5$, we used RR scheduling, respectively without and with obstacles. CF_1 remained static for all runs in each area. For each of the five areas shown in Fig. 2, five different scenarios were defined for each variant ($V1$ to $V5$), resulting in a total of 25 simulations per area, considering the methodology shown in Fig. 3. After simulating five different scenarios, for each of the six variants ($V0$ to $V5$) for the five areas (A_0 to A_4), we obtained $5 \times 6 \times 5 = 150$ sets of results, including the baseline ($V0$). The objective was to compare the results obtained from the $V0$ variant (without MIAB), with the other five different variants (with MIAB). The gain of the special team aggregate network capacity for each variant, expressed as a percentage of the aggregate network capacity of $V0$, was calculated as $(C_{Vx} - C_{V0}) \times 100 / C_{V0}$. The solver provided the aggregate network capacity of the special team, the gain percentage compared to $V0$, each $S_{u,m}^M$ or $S_{u,k}^F$, the backhaul capacity and the MIAB's position within each area. We then assessed the gains obtained for the aggregate network capacity of the special team as a function of the average topology distance (on the x-axis) and the inter-distance depicted by the red line (on the right y-axis), as depicted in Fig. 4 for area A_0 . The average topology distance is the average distance between the UEs and CF_1 . The inter-distance is the distance between the two UEs of the special team. Light blue bars show negative gains compared to $V0$, due to higher path loss attenuations caused by obstacle shadowing. Green bars, representing PF scheduling, show higher gains without obstacles, as expected. Similarly, brown bars, representing RR scheduling, show the highest gains, especially with obstacles, for greater distances. This is due to the higher availability of RBs for the special team, despite being limited by the backhaul, combined with higher spectral efficiencies but with the appropriate user associations. Moving right on Fig. 4, higher separation between network nodes results in even higher gains. By focusing on the gains (125 results, from $V1$ to $V5$) compared to $V0$, Fig. 5 depicts the cumulative distribution function (CDF) of each variant, for all the five scenarios of all the five areas studied. The light blue CDF confirms that obstacle shadowing typically causes a 50% reduction of the objective capacity. In most cases, RR is preferable to PF scheduling, except when obstacles are present ($V3$ and $V5$), where performance is similar. Nonetheless, the MIAB consistently introduces gains in the objective function, increasing the aggregate network capacity for the special team, even in the presence of obstacles.

The solver also calculated the backhaul capacity required to accommodate the combined network capacities of the UEs directly served by the MIAB, which might not necessarily have been part of the special team. This confirms that the cell selection was adequately chosen to maximise the aggregate network capacities of the special team.

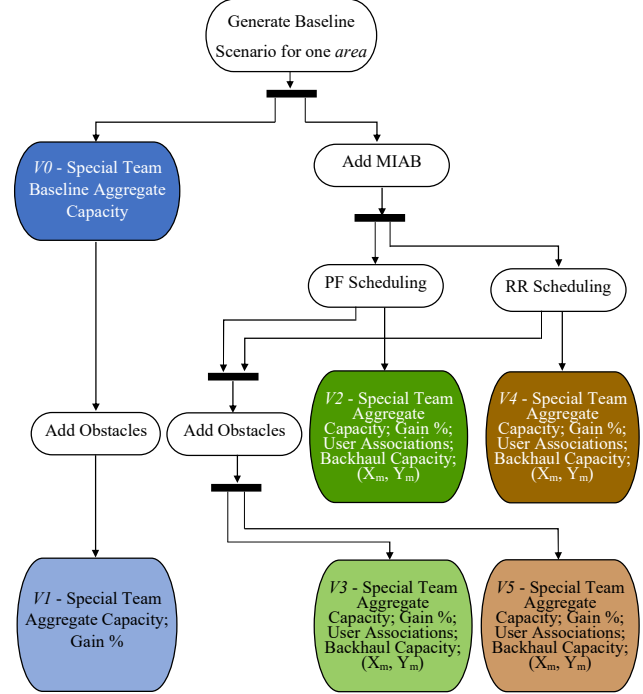


Fig. 3 – Methodology considered for network performance evaluation at each scenario. The coloured boxes summarise the results obtained for each variant ($V0$ to $V5$).

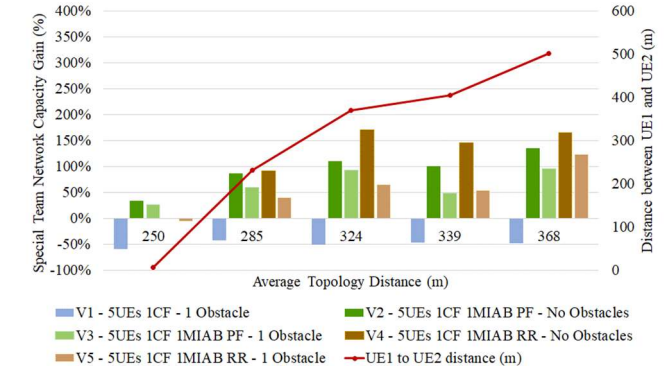


Fig. 4 - Aggregate network capacity gain percentages compared to the baseline $V0$, for the runs on A_0 .

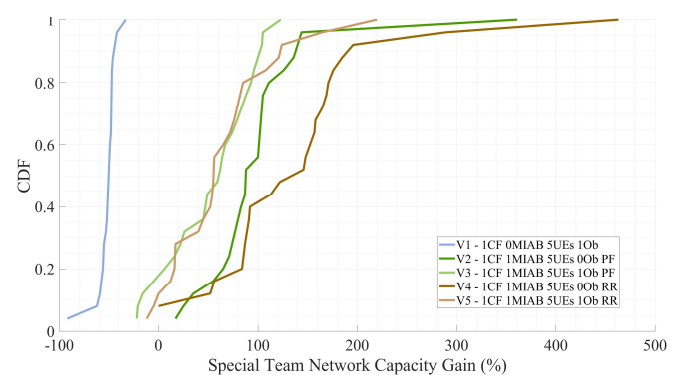


Fig. 5 - CDF of the aggregate network capacity gains for the special team.

Considering the backhaul capacity versus the aggregate capacity of the UEs served by the MIAB, Fig. 6 shows that the backhaul always supported the aggregate capacity for the UEs served by the MIAB, regardless of the variant. Table II provides the configuration parameter values.

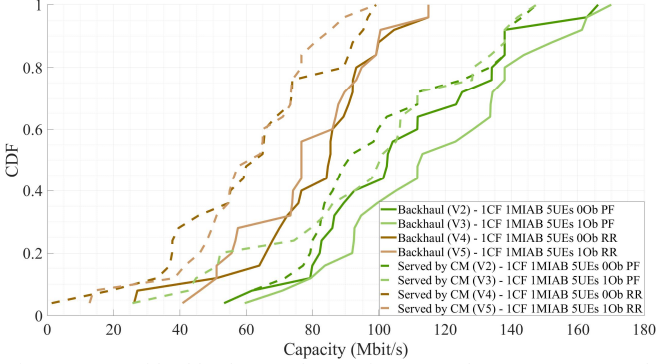


Fig. 6 - CDF of backhaul network capacity versus the aggregate network capacity of the UEs served by the MIAB.

TABLE II. PARAMETERS USED IN ALL THE RUNS OF THE SOLVER.

Parameter	Value
3GPP channel model	Urban Micro (UMi)
Number of MIABs and CFs, respectively	1 and 1
Number of UEs and special team	5 and 2 (UE1 and UE2)
Number of obstacles per scenario	1
MIAB's carrier frequency (GHz)	3.9
CFs' carrier frequency (GHz)	3.8
Numerology (μ fr1)	1
SCS (kHz)	30
Antenna model	Isotropic (SISO)
Transmission Power (dBm)	24
Bandwidth (MHz)	35.9
Thermal Noise PSD (dB)	-123.4
Traffic direction	Downlink
EESM Error Model	AMC with NrEesmCcT2
NR MAC Scheduler Types	OFDMA PF or RR
Number of RBs per slot	133
Number of Subcarriers per RB	9
Number of OFDMA symbols per slot	12

V. CONCLUSIONS

This paper proposes a system model formulated as an optimisation problem to determine the position of an MIAB including a performance evaluation study. The obtained MIAB's position maximises the aggregate capacity for a special team of UEs requiring improved network capacity within defined areas affected by significant obstacles. Our approach considers cell selection, the MIAB's backhaul capacity and two types of scheduling: PF and RR. The proposed solution allows for gains up to 200% for the 90th percentile, especially when using RR scheduling, while considering the impact of obstacle-induced shadowing. Moreover, the backhaul wireless link always supports the capacity provided by the MIAB to the served UEs. Through these contributions, we aim to support Mobile Network Operators in optimising the network planning of IAB networks for outdoor environments, such as seaports, which are typically characterised by multiple UEs, IAB donors, MIABs, and substantial obstacles. For future work, we plan to explore scenarios involving a greater number of UEs and MIABs, while autonomously controlling their locations using O-RAN xApps.

REFERENCES

- [1] C. A. Gizelis, et al., "Towards a Smart Port: The Role of the Telecom Industry" in *IFIP International Conference on AI Applications and Innovations*, 2020.
- [2] 3GPP, "TS 36.304 V16.2.0 R16".
- [3] H. Pan, et al., "Joint Power and 3D Trajectory Optimizations for UAV-Enabled Wireless Powered Communication Networks with Obstacles", *IEEE Transactions on Communications*, pp. Vol. 71, N°. 4, April 2023.
- [4] S. K. Vankayala, et al., "Deep Learning Based Proactive Handover for 5G/6G Mobile Networks using Wireless Information" in *IEEE Globecom Workshops: Workshop on Recent Trends of Internet of Softwarized Things - 5G&B (IEEE IoTST-5G&B)*, 2022.
- [5] M. Al-Quraan, et al., "Intelligent Blockage Prediction and Proactive Handover for Seamless Connectivity in Vision-Aided 5G/6G UDNs" in *James Watt School of Engineering, University of Glasgow, G12 8QQ, UK*, 2022.
- [6] T. Nishio, et al., "When Wireless Communications Meet Computer Vision in Beyond 5G", *IEEE Communications Standards Magazine*, 2021.
- [7] D. Korpi, et al., "Visual Detection-based Blockage Prediction for Beyond 5G Wireless Systems" in *Nokia Bell-Labs, Espoo Finland - 2nd 6G Wireless Summit*, Levi, Finland, 2020.
- [8] A. Prado, et al., "Proportionally Fair Resource Allocation considering Geometric Blockage Modelling for Improved Mobility Management in 5G" in *Technical University of Munich, Germany, Q2SWinet - October 24-28*, Montreal, QC, Canada, 2022.
- [9] M. K. Shehzad, et al., "Backhaul-Aware Intelligent Positioning of UAVs and Association of Terrestrial Base Stations for Fronthaul Connectivity", *IEEE Transactions on Network Science and Engineering*, vol. 8, no. 4, Oct-Dec 2021.
- [10] X. Li et al., "Efficient Optimal Backhaul-Aware Placement of Multiple Drone-Cells based on Genetic Algorithm", in *IEEE International Conference on Robotics and Biomimetics*, Dali, China, Dec 2019.
- [11] C. T. Cicek, et al., "Backhaul-Aware Optimization of UAV Base Station Location and Bandwidth Allocation for Profit Maximization", *IEEE Access*, vol. 8, 2020.
- [12] C. Qiu, et al., "Joint Resource Allocation, PLacement and User Association of Multiple UAV-Mounted Base Stations with In-Band Wireless Backhaul", *IEEE Wireless Communications Letters*, vol. 8, no. 6, 2019.
- [13] M. Nikooroo, et al., "Channel Reuse for Backhaul in UAV Mobile Networks with User QoS Guarantee" in *IEEE International Conference on Communications (ICC): Mobile and Wireless Networks Symposium*, 2023.
- [14] Y. Almoghaithawi, et al., "Optimal Location of Base Stations for Cellular Mobile Network considering changes in Users Locations", *Journal of Engineering Research*, Elsevier, 2024.
- [15] 3GPP, "TS 38.214 V16.5.0, Table 5.1.3.1-2".
- [16] 3GPP, "TR 38.901 V17.0.0 R17, Table 7.4.1-1".
- [17] S. Lagen, et al., "New Radio Physical Layer Abstraction for System-Level Simulations of 5G Networks - CTTc, Interdigital".
- [18] P. F. Correia, et al., "Positioning of a Next Generation Mobile Cell to Maximise Aggregate Network Capacity", *16th EAI International Conference on Simulation Tools and Techniques*, Dec 2024.
- [19] G. Y. Suk, et al., "Full Duplex Integrated Access and Backhaul for 5G NR: Analyses and Prototype Measurements", Yonsei University, Korea; Samsung Electronics Co., Ltd., Korea, 2022.